JOURNAL OF Materials CHEMISTRY

# Effect of surfactant type, substitution by aluminium and additives on direct liquid crystal templated monolithic silica

**Jacques Rozière, Markus Brandhorst, Roger Dutartre, Mélanie Jacquin, Deborah J. Jones,* Pierre Vitse and Jerzy Zajac**

*Laboratoire des Agrégats Moléculaires et Matériaux Inorganiques, UMR 5072, Université Montpellier 2, Place E. Bataillon, 34095 Montpellier cedex 5, France*

***Received 15th June 2001, Accepted 16th August 2001***
***First published as an Advance Article on the web 7th November 2001***

A range of monolithic silicas and aluminosilicates with disordered crystalline-like pore structures and high surface areas have been synthesised based on a direct crystal templating approach to surfactant-assisted sol–gel synthesis of porous materials. Commercially available oxyethylated non-ionic surfactants, including sorbitan-based molecules and those possessing a straight alkyl or alkylphenol tail, were used as structure-directing agents in high-concentration surfactant solutions (about 50 wt%). Incorporation of aluminium into monolithic silica increases pore wall thickness. Thermoprogrammed desorption of ammonia in the temperature range from 373 K to 923 K was used for the evaluation of the number and the strength distribution of surface acid sites. The mean strength of acid sites reaches a maximum value for the material prepared with a Si : Al ratio of 20, as evidenced by flow-microcalorimetry measurements of ammonia chemisorption at 373 K. The calcined silica and aluminosilicate materials were characterised by nitrogen gas adsorption at 77 K. The mean pore diameter ranges from 2 nm to 4 nm. The addition of lithium nitrate and 1,3,5-trimethylbenzene to the reaction mixture was investigated to prepare materials with mesopores up to 6 nm. Mean pore diameters increase with increasing length of the hydrophobic tail of the template, decreasing number of oxyethylene units, increasing amount of lithium nitrate or hydrophobic solubilisate added to the reaction mixture, and decreasing synthesis temperature. The pore size appears to be sensitive to the orientation of the polyoxyethylene chain within the aqueous domains of the lyotropic mesophases as a result of its interaction with the growing inorganic precursor units.

## Introduction

It has long been an operational premise that supramolecular surfactant or polymer aggregates can direct the structures of oxides leading to nanostructured materials with controllable pore sizes and shapes.[1–9] Periodic mesoporous silica and aluminosilicates of the MCM type are the primary examples of solids prepared based on non-covalent interactions between the surfactant template and the matrix.[10–22] There is now a very large and growing literature dealing with the sol–gel synthesis of regular silica–surfactant mesophases. Two distinct approaches emerge from discussions about the templating pathway.[7,23]

By far the most often encountered approach utilises low-concentration surfactant solutions and the mesophases are formed through structure-directing electrostatic, van der Waals, or hydrogen-bonding interactions between surfactant micelles and inorganic precursor units. Such a co-operative self-assembly can occur by electrostatic charge-matching, $S^+I^-$, between the cationic amphiphile $S^+$ and the inorganic polymer $I^-$, by a counterion-mediated mechanism, $S^+X^-I^+$, where $X^-$ is the mediating ion, or by an electrically neutral pathway, $S^0I^0$, with the use of a non-ionic surfactant $S^0$.[7,24–26] Solution $S^0I^0$ assembly of mesoporous silica has been achieved by using commercial non-ionic surfactants on the suggestion that rod- or worm-like micelles template the formation of the regular ceramic nanostructures.[27–30] The resulting mesoporous materials exhibit a less regular long-range order, as evidenced by a single X-ray diffraction peak.[27,28] However, non-ionic systems have weaker assembly forces which lead to thicker matrix walls and increase the thermal stability of the final porous structure.

A second approach to the preparation of regular mesoporous silica is based on the direct liquid crystal templating pathway.[23] In simple surfactant–water systems, lyotropic liquid crystals with cubic, hexagonal or lamellar geometry are commonly found as single phases in surfactant phase diagrams, usually at surfactant concentrations above about 40% by weight.[31–33] In general, significant water contents correspond to both bound and unbound water molecules in polar regions separating the surfactant head-groups,[34] where the water-soluble units of the inorganic precursor may be dissolved. Thus the polycondensation process is probably confined to the aqueous domains of a liquid-crystalline phase.[23,35] Since the surfactant aggregates are encased in the inorganic matrix during solidification, macroscopic nanostructured monoliths of desirable shape and size can be obtained. The resulting nanostructure is dictated only to a limited extent by the reagents and the synthetic conditions, providing that the addition of the preursor does not move the positions of the boundaries and the relative sizes of the various liquid crystalline phases. The existence of the birefringent liquid crystalline phase during the solidification of the inorganic matter may be readily demonstrated in the polarising microscope or by low-angle X-ray diffraction.[35–37]

The first attempts made by Friberg and co-workers[38,39] at the templating of an inorganic sol–gel medium in lyotropic liquid-crystalline phases drew attention to the role of methanol or ethanol evolved during hydrolysis of the silica precursor (silicon alkoxides) in destroying the lyotropic liquid-crystalline order. In more recent work, the isotropic character of the surfactant–water–silicic acid mixture in the presence of alcohol is exploited at the first stage of the synthesis, where it allows the reaction mixture to be well homogenised.[23]

An effective approach to regular mesoporous nanostructures in lyotropic liquid-crystalline phases involving the use of high concentrations of non-ionic amphiphiles was proposed by

 DOI: 10.1039/b105276b

**Table 1** Non-ionic surfactants used in the preparation of monolithic silicas and aluminosilicates

| Trade name | Manufacturer | Approximate formula | Designation |
|---|---|---|---|
| Brij 30 | Aldrich | $C_{12}H_{25}O(CH_2CH_2O)_4H$ | B30 |
| Brij 52 | Aldrich | $C_{16}H_{33}O(CH_2CH_2O)_2H$ | B52 |
| Tergitol 15-S-9 | Sigma | $C_{11-15}H_{23-31}O(CH_2CH_2O)_9H$ | T9 |
| Montanox 20 | SEPPIC | Sorbitan.20EO.monooleyl ester | M20 |
| Montanox 80 | SEPPIC | Sorbitan.20EO.monolauryl ester | M80 |
| Montanox 85 | SEPPIC | Sorbitan.20EO.trioleyl ester | M85 |
| Octylphenol-10EO | SEPPIC | $p$-$C_8H_{17}C_6H_4O(CH_2CH_2O)_{10}H$ | OPE10 |
| Nonylphenol-*n*EO | SEPPIC | $p$-$C_9H_{19}C_6H_4O(CH_2CH_2O)_nH$ $n=4,5,8,10,12$ | NPE*n*, *e.g.* NPE4 |
| Dodecylphenol-*n*EO | SEPPIC | $p$-$C_{12}H_{25}C_6H_4O(CH_2CH_2O)_nH$ $n=4,5,7,10$ | DPE*n*, *e.g.* DPE5 |
| Lauryl ether-*n*EO | SEPPIC | $C_{12}H_{25}O(CH_2CH_2O)_nH$ $n=2,4,8$ | DE*n*, *e.g.* DE8 |

Attard *et al.*[36,37] Octaethylene glycol monododecyl and monohexadecyl ethers were employed to template the synthesis of mesoporous silica, and tetramethyl orthosilicate (TMOS) served as the silica precursor. The resulting silica phase was a cast of the organic mesophase, retaining its mesoporous structure after removal of the surfactant by calcination and showing cracks due to the structure shrinkage.

The direct liquid crystal templating approach was also studied by other researchers.[40–49] With polyoxyethylenated straight-chain alcohols as the directing agents, Ammundsen *et al.*[41] obtained silica monoliths with a disordered hexagonal pore arrangement, by carrying out the synthesis in a high-concentration surfactant solution. Göltner *et al.*[42] described the preparation of mesoporous monolithic silica either from amphiphilic block copolymers or from octaethylene glycol monohexadecyl ether at high template concentrations. Tolbert *et al.*[43] used the cationic surfactant cetyltrimethylammonium bromide at moderate concentrations as the template. They achieved a long-range alignment of hexagonal silicate-structure mesophases, by applying a high magnetic field. This alignment was preserved after polymerisation of the silicate species by acid treatment. Wei *et al.*[44,45] reported the preparation of mesostructured monolithic silica from tetraethoxysilane (TEOS) precursor, by using NaOH to catalyse the hydrolysis of TEOS and the polycondensation in the presence of D-glucose at high concentrations as a non-surfactant template. The latter was subsequently removed by extraction with water under mild ambient conditions. More recently, the direct liquid crystal templating approach was also used to prepare monolithic silica from TMOS or TEOS in block copolymer–water solutions mixed with alcohol co-surfactants and some hydrophobic swelling agents, like cyclohexane or octane.[46–48] Microemulsion mesophases with long-range ordering were also proposed for the formation of silica monoliths.[49] In the present paper, the results of long-term and systematic studies undertaken on the preparation of lyotropic mesophase templated mesoporous silicate and aluminosilicate nanostructures are reported. The main emphasis is on the application of polyoxyethylenated nonionic surfactants as cheap template sources. These amphiphiles include sorbitan-based molecules and those possessing a straight alkyl or alkylphenol tail. The length of the alkyl moiety or that of polyoxyethylene chain can be modified to give a wide range of templates varying in solubility in aqueous media. The complete phase diagrams for such species are usually known and show most of the major types of lyotropic mesophase which are commonly encountered in surfactant–water systems.[33,50]

The intention of the present work is to demonstrate the effect of the surfactant molecular structure upon the porosity of the templated monoliths. The influence on textural properties of the temperatures at which polycondensation, vacuum treatment and drying are performed, and the addition of group I metal salts and hydrophobic solubilizates is studied. The incorporation of Al heteroatoms into the silica matrix was also undertaken in order to enhance the surface acidity of the nanostructured monoliths.

## Experimental

### Chemicals

The polyoxyethylenated non-ionic surfactants used are listed in Table 1, together with the trade name, the manufacturer, the approximate chemical formula, and the acronym or abbreviation, which will be used afterwards. The value of $n$ in Table 1 represents the average number of ethylene oxide units per molecule of surfactant.

Tetraethoxysilane, $Si(OCH_2CH_3)_4$, and 1,3,5-trimethylbenzene, $C_6H_3(CH_3)_3$, were purchased from Fluka, whereas aluminium nitrate nonahydrate, $Al(NO_3)_3{\cdot}9H_2O$, lithium nitrate, $LiNO_3$ and a 65% nitric acid solution were obtained from Aldrich. Gaseous ammonia, nitrogen and helium of ultra high purity were supplied by Air Liquide (France).

### Syntheses

Commonly, monolithic silica can be prepared under conditions of slow hydrolysis of the precursor precluding a rapid precipitation of coarse-size powders. Tetraethoxysilane (TEOS) was employed as silica precursor. The molar ratio TEOS : water was 1 : 4. The lyotropic liquid crystal templating approach employed in the present study required the surfactant to be used in high concentrations (about 50 wt%). A dilute 0.1 M $HNO_3$ aqueous solution served as both solvent and pH regulator.

A typical synthesis of pure silicate involved stirring of the surfactant with dilute $HNO_3$ followed by the addition of TEOS, and further stirring until a complete dissolution of the reagents was achieved. The system was maintained at constant temperature (usually at 30 °C) by means of a water bath. Ethanol produced by the reaction was removed by vacuum treatment at room temperature for 2 h, and then the gelling mixture was left to dry in an oven at 25 °C. A three-day period was usually sufficient to allow solid phase condensation to occur and water and residual ethanol to evaporate. The as-synthesised samples were calcined at 560 °C for 10 h. These materials are designated MO-Si*TA*, where *TA* refers to the surfactant used in the synthesis. Therefore, a material prepared in the presence of nonylphenol-8EO is designated MO-Si*NPE8*.

Adaptations of the above procedure were performed through the introduction of aluminium nitrate to dilute $HNO_3$ prior to addition of surfactant and TEOS, using Si : Al molar ratios of 10, 20, 40, whereas lithium nitrate or 1,3,5-trimethylbenzene (TMB) were added after all other reagents. The resulting materials are named MO-SiAl*x*TA, where $x$ is the mole ratio Si : Al and *TA* refers to the surfactant template.

### Characterisation

X-Ray powder diffraction data were recorded on an automated Philips X'Pert diffractometer with Cu K$\alpha$ radiation. The coordination environment of aluminium in representative calcined phases was examined with a Bruker ASX400 solid state NMR spectrometer. Transmission electron micrographs were obtained with a JEOL 1200 EX microscope operating at 100 kV. Adsorption–desorption of nitrogen at 77 K was investigated using an automated volumetric Analsorb 9011 apparatus. Prior to the adsorption measurements, all samples were evacuated to $10^{-5}$ Torr at 220 °C for 12 h. A complete adsorption isotherm, followed by a desorption isotherm, was obtained with 20–30 points on each branch. BET plots were constructed below a relative pressure of 0.2 from the adsorption branches, the linear part of the BET plot being extended to $P/P_0 = 0.3$ for samples containing larger mesopores. These lines were subsequently used to evaluate the BET specific surface area, $S_{BET}$, taking a cross-sectional area of 0.162 $nm^2$ per nitrogen molecule. Determination of surface acidity was based on thermoprogrammed desorption of ammonia. Samples were pre-treated in a nitrogen flow of 30 ml $min^{-1}$ at 723 K for 4 h and then saturated in an ammonia flow of 30 ml $min^{-1}$ at 373 K. To completely remove the $NH_3$ molecules physisorbed on the surface, nitrogen carrier gas was subsequently flowed through the sample at the rate of 30 ml $min^{-1}$ at 373 K for 4 h. Ammonia desorption between 373 and 923 K (heating rate 10 K $min^{-1}$) was analysed using an on-line conductivity cell with a HCl solution for trapping the effluent gases. The mean strength of ammonia chemisorption at 373 K was measured with a 4Vms Microscal Flow Microcalorimeter. Solid samples were first outgassed at 373 K overnight in the calorimetric cell and then flushed with a helium flow of 2 ml $min^{-1}$ for 4 h. The flow of carrier gas was subsequently stopped and replaced by a stream of pure ammonia flowing at the same rate. The progress of adsorption was continuously monitored by the evolution of heat measured by thermistors sensing temperature changes in the adsorbent bed and, simultaneously, adsorbate transfer from the gas phase to the solid–gas interface was monitored by measuring composition changes in the effluent leaving the adsorbent and passing through a thermal conductivity (TC) detector. Desorption of physically adsorbed $NH_3$ molecules was performed by interchanging the supply of ammonia with the original flow of helium carrier gas at the same temperature of 373 K. Calibration of the areas under the thermal peaks was carried out by dissipating a known amount of energy in the cell under the same flowing conditions (Joule heating using a calibration probe incorporated into the outlet tube) and integrating the related exothermic peak. The TC detector calibration factor was determined from the injection of 500 µl of pure ammonia into the stream of helium carrier gas percolating through the detector.

## Results and discussion

The ability to form macroscopic nanostructured monoliths is of importance for the formation of porous materials with desired size and shape without compromising the large surface area and pore volume. Optically transparent and crack-free silica objects may be simply made in a mould. The photograph of a monolithic disc of 15 mm in diameter and 3 mm thick is shown in Fig. 1.

It should be noted that commercial non-ionic surfactants can be complex mixtures of products with a certain distribution of polyoxyethylene chain lengths. In consequence, such mixtures may form two-phase regions, which consist of lamellar or hexagonal mesophases of the main amphiphilic constituent dispersed in an isotropic solution containing monomers or single micelles of the other surfactant homologues.

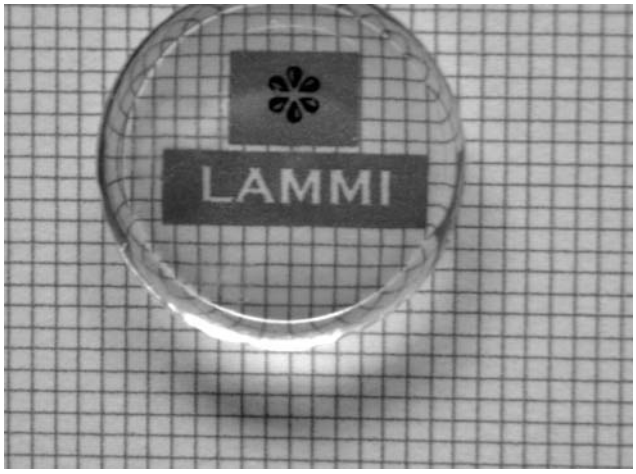


**Fig. 1** Photograph of a monolithic silica disc prepared using B30 as a structure-directing agent.

Alternatively, the formation of mixed mesomorphic phases is to be envisaged. In both cases, one should expect monolithic materials with a less regular porous network.

### Pure silica monoliths

It is known[51] that the size and shape of surfactant self-assemblies depend on the nature of both hydrophobic tail and hydrophilic head-group. In agreement with common geometric considerations, the textural parameters of monolithic silicas should be modified with changes in the molecular structure of the template. To verify this hypothesis, various oxyethylated amphiphiles were used in the synthesis at similar concentrations (about 50 wt%).

The X-ray diffraction patterns of calcined monolithic silicas prepared using three directing agents with the same hydrophobic moiety $C_{12}$, namely B30, DE2 and M80, are shown in Fig. 2. These curves are representative of purely siliceous materials synthesised in lyotropic liquid crystalline phases of polyoxyethylated non-ionic surfactants. In the range up to 10° $2\theta$, only a single diffraction peak is observed. This X-ray diffraction pattern is different from those reported on MCM-41 type materials,[10–20] where lines corresponding to Miller indices (100), (110), (200) and (210) are generally observed. X-Ray patterns with only one first-order scattering peak were

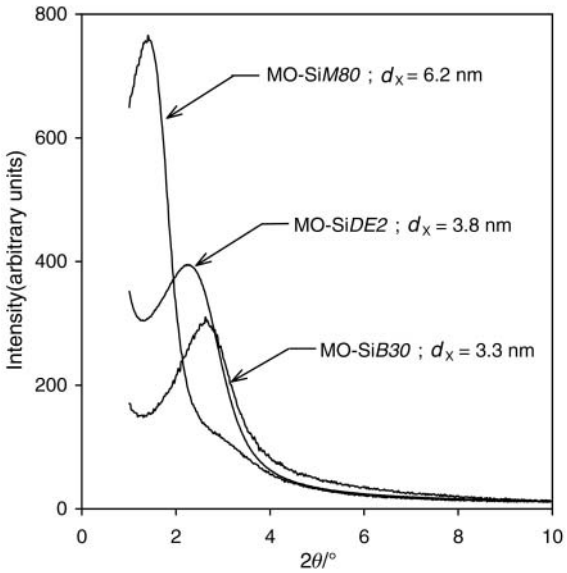


**Fig. 2** Powder XRD patterns of calcined MO-Si*TA* silicas prepared with various structure-directing agents.

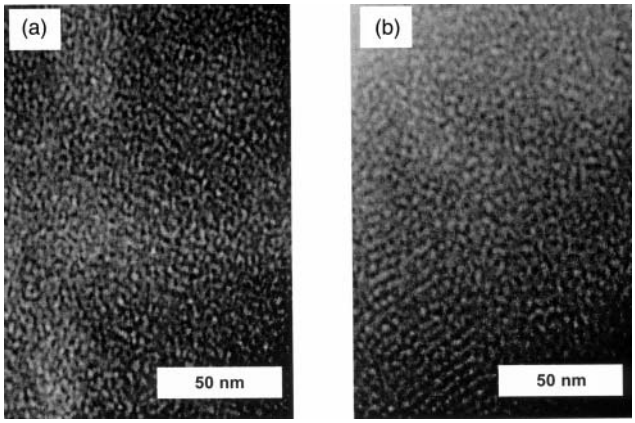


**Fig. 3** TEM micrographs of calcined MO-Si*TA* silicas prepared using B30 (a) and M85 (b) as structure-directing agents.

also obtained by Pinnavaia *et al.*,[27,28] who investigated the assembly of mesoporous silica based on polyoxyethylated non-ionics as structure directors in low-concentration surfactant solutions. These authors suggested that the lack of higher order Bragg reflections does not exclude the existence of local hexagonal symmetry. If the size of scattering domains is small, no high-order reflections can be monitored in the small-angle X-ray diffractograms. When the solidification of the inorganic matrix is templated by non-ionic micelles at low surfactant concentration, weak directional forces operating between surfactant self-assemblies and growing inorganic clusters are not capable of inducing the formation of liquid crystalline aggregates. Under such circumstances, highly structured alignment of uniform pores in the calcined materials is unlikely. The XRD patterns of the calcined monolithic silicas shown in Fig. 2 can rather be attributed to crystalline-like porous structures being less ordered, where the polydispersity of non-ionic templates may be responsible for such disorder. This conclusion is consistent with the TEM images presented in Fig. 3, where regions showing different structural features can be observed.

The X-ray Bragg spacing, $d_X$, is clearly dependent on the chemical structure of the template, indicating that the surfactant mesophases play an important role in the formation of monolithic nanostructures. Among the three non-ionic amphiphiles, sorbitan-based M80 has a bulky hydrophilic head-group containing 20 EO units. The $d_X$-value of the monolithic silica, prepared using this structure-directing agent, is almost twice those of the two other materials.

The study of the pore structure of micro- and mesoporous solids is closely connected with the interpretation of adsorption–desorption isotherms of gaseous adsorptives, notably those of nitrogen at 77 K. With certain precautions, which will be discussed hereafter, it is possible to analyse such curves so as to obtain a reasonable estimate of the specific surface and an approximate assessment of the pore size distribution. The essential features of nitrogen adsorption isotherms measured on a variety of representative calcined monolithic silicas templated with polyoxyethylated non-ionic surfactants are indicated in Fig. 4.

Commonly, there is a distinct step in the adsorption isotherm on a highly ordered porous substrate and a qualitative indication of the homogeneity of the pore size distribution is provided by the steepness of this adsorption step. The extended transition regions clearly seen in the adsorption curves in Fig. 4 may be ascribed to a certain heterogeneity of porous structures. For B30, M85 and M20 used as structure-directing agents, the phenomenon of $N_2$ adsorption is completely reversible, and the corresponding desorption isotherms have not been reported. Each of the three adsorption curves has a steep initial portion and a well-defined horizontal plateau at

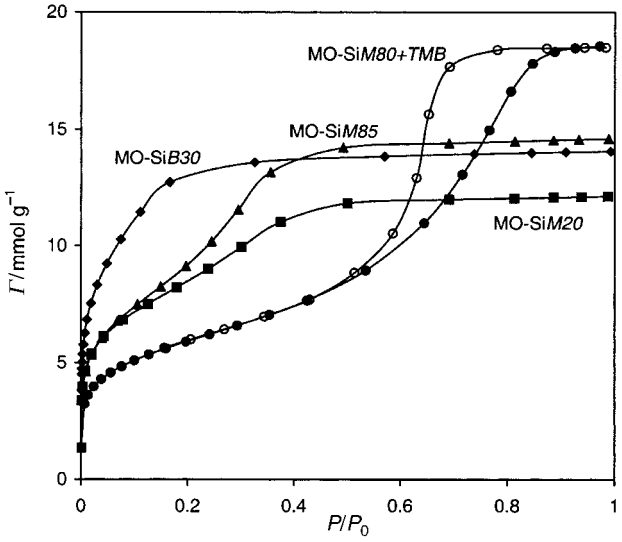


**Fig. 4** Adsorption–desorption isotherms of nitrogen at 77 K onto calcined MO-Si*TA* silicas prepared with various structure-directing agents. TMB denotes 1,3,5-trimethylbenzene solubilisate added to the reaction mixture so as to swell the templating liquid-crystalline phase.

larger relative pressures, two characteristic features of a type I isotherm. Nevertheless, a gradual increase in the amount of $N_2$ adsorbed at low and moderate relative pressures suggests that these materials contain small mesopores, in addition to micropores. For the three monolithic silicas analysed here, the quantity of nitrogen adsorption practically levels off below a relative pressure of about 0.42 and, consequently, the experimental adsorption isotherm cannot possess the hysteresis loop characteristic of cylindrical pores open at both ends or of parallel-sided slits.[52] The majority of adsorption isotherms resulting from physical adsorption of nitrogen onto the non-ionic-templated monolithic silicas studied in the present paper are similar in shape to these three curves, indicating that their pore size is limited to about 4 nm.

An alternative approach to increasing the pore size based on the addition of sparingly water-soluble substances to the surfactant solution has been exploited in the present study. In dilute surfactant solutions, molecules that are nonpolar or not easily polarisable are located in the inner core of the micelle between the ends of the hydrophobic groups of the surfactant monomers, whereas more polar molecules are solubilised mainly in the outer regions of the micellar structures.[53,54] With the incorporation of solubilisate into a micelle, the size and shape of the micelle may change considerably. This effect is well evidenced in Fig. 4 by the type IV isotherm with a hysteresis loop measured on a monolithic sample templated with M80 in the presence of 1,3,5-trimethylbenzene (TMB). Calcined silica MO-Si*M80 + TMB* is thus a typical mesoporous adsorbent with a high pore volume and a small external surface area. At higher relative pressures, the adsorption and desorption branches are not parallel to each other. This probably means that the body of some pores is tapered which gives rise to 'pore blocking' effects during desorption.[55]

### Surface area and pore structure parameters

Plots of pore size distribution can give useful indications of significant differences between pore systems in a related set of solids. Fig. 5 presents a few examples of the distributions derived from the four isotherms shown in Fig. 4. Since MO-Si*B30* seems to be a predominantly microporous solid, its pore size distribution was determined in the pressure range up to 0.2 based on the Horwath–Kawazoe (HK) method for cylinder pore geometry,[56] (see Fig. 5*a*). The most probable pore diameter is about 0.9 nm. The distribution is, however,

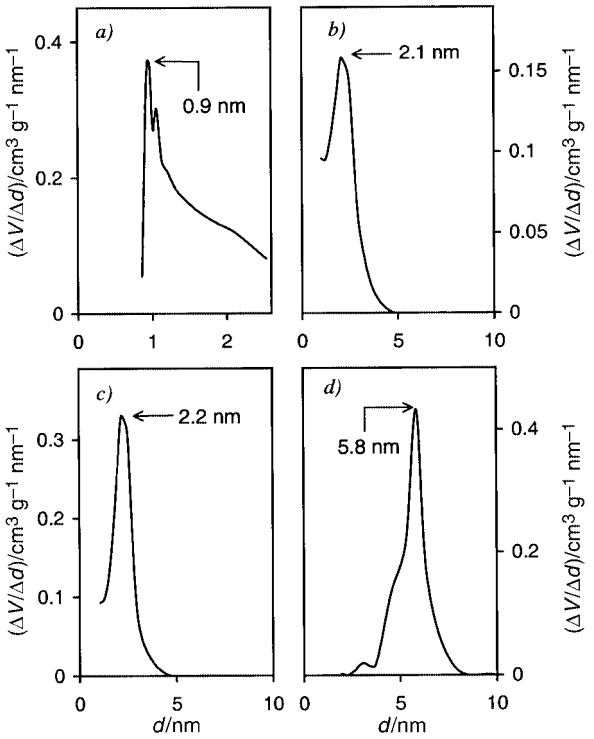


**Fig. 5** Pore size distributions derived from the nitrogen adsorption isotherms shown in Fig. 2: *a*) Horwath–Kawazoe distribution for fine pore MO-Si*B30*, *b*) BJH distribution for MO-Si*M20*, *c*) BJH distribution for MO-Si*M85*, *d*) BJH distribution for a monolithic silica templated with M80 in the presence of 1,3,5-trimethylbenzene (Si : TMB = 1) calculated from the desorption branch of the hysteresis loop. The numbers refer to the most probable values of pore diameter.

right-skewed, which means that there is a significant contribution from larger pores. Furthermore, the cumulative pore volume predicted by the HK method is only a small fraction of the overall amount of $N_2$ adsorbed. As a result, one can expect the mean pore diameter to be shifted towards the mesopore size range. For the remaining three samples, the classical method developed by Barrett, Joyner and Halenda (known as the BJH method with the Halsey thickness equation[52]) could be applied. Fig. 5*b*, *c* and *d* provide an illustration. In the case of MO-Si*M85* and MO-Si*M20*, the most probable pore diameter is located at the lower end of the mesopore size range. Nevertheless, it should be remembered that the BJH method is known to systematically underestimate the pore size.[57] The BJH distributions are quite narrow, but they describe only a part of the porous structure. The HK distributions calculated for these materials reveal non-negligible contributions from micropores with a diameter ranging between 1 and 2 nm. The situation is thus more complicated since the micropore and mesopore ranges appear to overlap. In conclusion, the overall pore structure in monolithic silicas templated with oxyethylated non-ionic surfactants is to a certain extent heterogeneous, which is consistent with the conclusion drawn from the analysis of the XRD diffractograms and TEM images in Fig. 2 and 3.

For monolithic material MO-Si*M80+TMB*, the BJH distribution calculated from the desorption branch of the isotherms of nitrogen is shown in Fig. 5*d*. The curve is centred about a pore diameter of 5.8 nm, indicating that the addition of the solubilisate to the surfactant phase is of major practical importance for the templating mechanism and the control of porosity. It should be mentioned that the pore size distribution curve derived from the adsorption branch of the isotherm gave a different picture of the pore structure: the BJH distribution was broader and the most probable value of pore diameter was equal to 6.2 nm. Therefore, in pores with a tapering body where network effects are known to be present, the distribution curve based on the desorption branch of the hysteresis loop is likely to give a somewhat misleading picture of the pore structure.

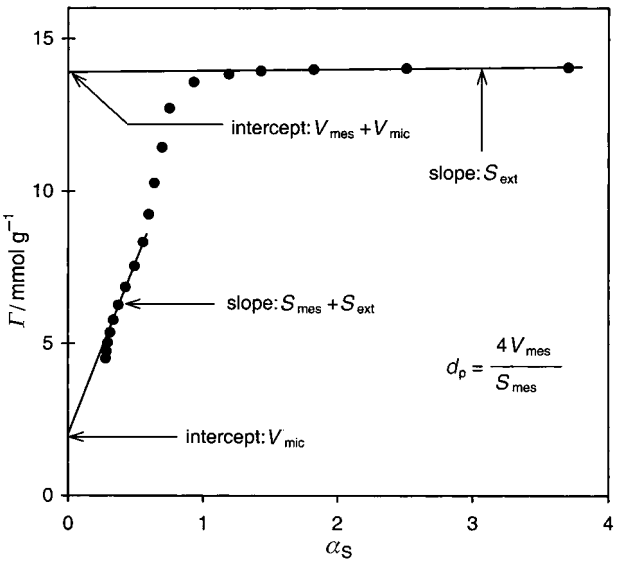


**Fig. 6** $\alpha_S$-plot for the adsorption of nitrogen at 77 K on a sample of MO-Si*B30* with a BET surface area of 1118 $m^2 g^{-1}$. The slopes and intercepts of two linear parts are used to determine the mesopore surface area and volume, $S_{mes}$ and $V_{mes}$, the external surface area, $S_{ext}$, and the micropore volume, $V_{mic}$. The mean pore diameter, $d_p$, is calculated assuming a cylindrical pore shape.

In order to investigate the effect of the template structure on the textural characteristics of monolithic silica, a simplified comparison criterion may be founded on the BET specific surface area, $S_{BET}$, and certain parameters describing the 'average' pore structure. Despite difficulties of interpretation,[57] the experimental adsorption isotherms of nitrogen at 77 K were analysed to obtain estimates of these parameters.

The standard $\alpha_S$ curve, determined on a non-porous hydroxylated silica,[52] was used to produce $\alpha_S$ plots from the adsorption branches. An example is shown in Fig. 6, where various linear portions are used to calculate the micropore volume, $V_{mic}$, the area of the mesopore walls, $S_{mes}$, the external surface, $S_{ext}$, and the volume of mesopores, $V_{mes}$. The mean pore diameter, $d_p$, was calculated from the ratio between the mesopore volume, $V_{mes}$, and the mesopore surface area, $S_{mes}$, assuming a cylindrical pore shape. Since the micropore shape is not precisely known, the average pore width and the area of the micropore walls cannot be calculated. For MO-Si*M80+TMB*, a straight line through the origin resulted, pointing to the absence of micropores in this material.

The parameters determined for the selected samples are given in Table 2. The mean pore diameters are different from the most probable values, as determined from the appropriate distribution curves presented in Fig. 5. The differences can be certainly ascribed to a certain heterogeneity of the pore structure, but also to dependence of these parameters on the underlying theoretical models. So far as the 'average' pore network is concerned, the monolithic silicas are mesoporous solids with a very small external surface area.

**Table 2** Surface area and porous structure parameters of some monolithic silicas prepared with various directing agents

| Sample | $S_{BET}$/ $m^2 g^{-1}$ | $S_{mes}$/ $m^2 g^{-1}$ | $V_{mes}$/ $cm^3 g^{-1}$ | $d_p$/ nm | $V_{mic}$/ $cm^3 g^{-1}$ |
|---|---|---|---|---|---|
| MO-Si*B30* | 1118 | 731 | 0.41 | 2.3 | 0.07 |
| MO-Si*B52* | 940 | 584 | 0.45 | 3.1 | 0.07 |
| MO-Si*M20* | 697 | 463 | 0.35 | 3.0 | 0.06 |
| MO-Si*M85* | 767 | 499 | 0.45 | 3.6 | 0.05 |
| MO-Si*M80+TMB* | 484 | 476 | 0.63 | 5.3 | 0.00 |

Within the Brij template series, lengthening of the hydrophobic moiety causes an increase in the mean pore diameter and a decrease in the surface area (both $S_{BET}$ and $S_{mes}$) of the resulting monolithic silicas. The mesopore volume increases a little, whereas the value of $V_{mic}$ seems to be unchanged. The addition of extra hydrophobic moieties to the surfactant structure in the Montanox template family appears to increase markedly the mean pore diameter and the mesopore volume of the calcined material. These changes are accompanied by a slow increase in the surface areas. Among the five monoliths considered, fine pore MO-Si*B30* has the greatest surface area of about 1100 $m^2 g^{-1}$. The maximum mesopore volume and the minimum specific surface area are attained for predominantly mesoporous MO-Si*M80*+*TMB*.

### Aluminium silicates

Although the presence of salts in aqueous solution influences to a great extent self-assembly of ionic surfactants and can modify the general disposition of mesomorphic phases in the phase diagram, the effects appear to be small in the case of polyoxyethylated non-ionics.[51] It is thus probable that adding a salt of $Al^{3+}$ does not destroy the liquid-crystalline character of the surfactant phase. Based on this hypothesis, the introduction of aluminium into the framework of monolithic silica was programmed in the initial synthesis stage by mixing aluminium nitrate with a dilute acid solution, followed by the addition of an appropriate directing agent. The intention of this study was to incorporate aluminium sites into a silica matrix so as to enhance the surface acidity of the resulting samples, while maintaining the large surface area and pore volume. The aluminosilicate samples were prepared with a high surfactant concentration of about 50 wt%. The use of lyotropic surfactant templates for the synthesis led to macroscopic, transparent monoliths.

The X-ray diffraction patterns of calcined monolithic silicate and three aluminosilicates prepared using B30 and Si : Al molar ratios of 40, 20 and 10 are shown in Fig. 7. As in the case of purely siliceous samples, small-angle X-ray diffractograms with only one first-order scattering peak are observed. Clearly, aluminium addition leads to a shift of the peak maximum towards lower angles. In previous reports on aluminosilicate MCM-41,[20] incorporation of aluminium was shown to affect the pore wall thickness and not the pore diameter. The $d_X$ spacing, calculated from the first-order scattering peak, is

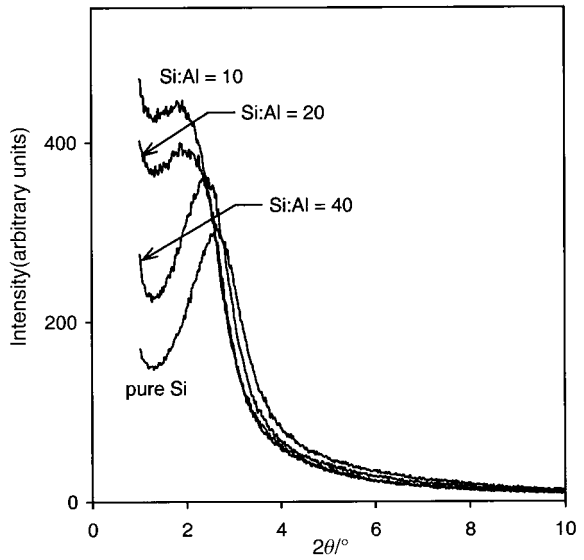


**Fig. 7** Powder XRD patterns of calcined silicate MO-Si*B30* and calcined aluminosilicate MO-SiAl*xB30* prepared with various molar Si : Al ratios.

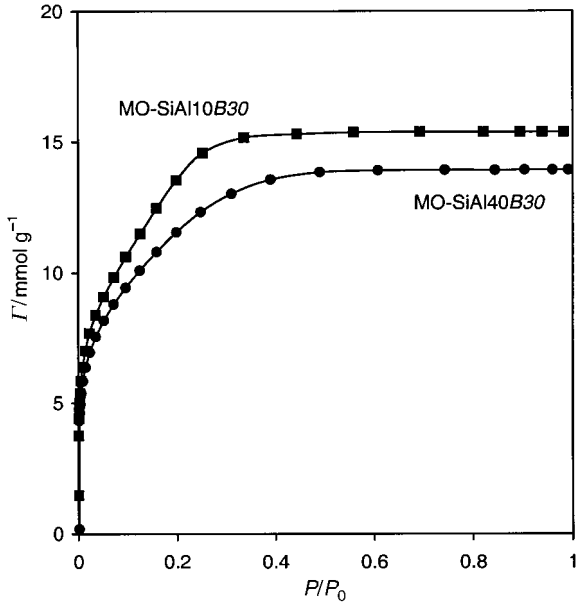


**Fig. 8** Adsorption isotherms of nitrogen at 77 K onto calcined MO-SiAl*xB30* samples prepared with Si : Al molar ratios of 40 and 10.

3.3 nm for the purely siliceous sample and it increases from 3.6 nm (Si : Al = 40) to 4.6 nm (Si : Al = 10) upon increasing aluminium content. Broadening of the peaks with decreasing Si : Al ratio can be attributed to less well-ordered structures. Therefore, the introduction of aluminium into silica monoliths contributes to the overall heterogeneity of the internal nanostructure, which does not remain unchanged as the aluminium content increases using a constant concentration of the structure-directing agent.

Fig. 8 presents the nitrogen adsorption isotherms for calcined aluminosilicate products prepared from the same surfactant B30 and with two different aluminium contents. The phenomenon of $N_2$ adsorption is completely reversible. The adsorption curve for MO-SiAl20*B30* is almost identical to that obtained on MO-SiAl10*B30* and hence it has not been reported in Fig. 8. Both curves are characteristic of materials with small pores and a gradual increase in the amount adsorbed in the range of low relative pressures means that the porosity is heterogeneous. The values of the BET specific surface area and the pore structure parameters are given in Table 3. It can be seen that the three aluminium materials possess practically the same 'average' pore network, with the surface area and pore volume being somewhat decreased with decreasing Si : Al ratio. This confirms again the trends obtained on incorporating Al into MCM-41 powders. The mean pore size of the monolithic aluminosilicates is greater than that of MO-Si*B30*. The comparison of the mean pore diameter with the $d_X$ spacing allows the averaged thickness of pore walls to be estimated: 1.0 nm, MO-Si*B30*; 0.9 nm, MO-SiAl40*B30*; 1.8 nm, MO-SiAl20*B30*; 2.0 nm, MO-SiAl10*B30*. As a consequence of the upward trend of wall thickness with Al content, the thermal and mechanical

**Table 3** Structural and surface properties of silicate and aluminosilicate monoliths prepared with B30 and various molar Si : Al ratios

| Sample | Si : Al = 10 | Si : Al = 20 | Si : Al = 40 | Si : Al = ∞ |
|---|---|---|---|---|
| $d_X$/nm | 4.6 | 4.4 | 3.6 | 3.3 |
| $S_{BET}$/$m^2 g^{-1}$ | 957 | 999 | 1159 | 1118 |
| $S_{mes}$/$m^2 g^{-1}$ | 647 | 661 | 684 | 731 |
| $V_{mes}$/$cm^3 g^{-1}$ | 0.42 | 0.43 | 0.46 | 0.41 |
| $d_p$/nm | 2.6 | 2.6 | 2.7 | 2.3 |
| $V_{mic}$/$cm^3 g^{-1}$ | 0.06 | 0.06 | 0.08 | 0.07 |
| $n_{acid}$/μmol $m^{-2}$ | 0.78 | 0.47 | 0.16 | 0.03 |

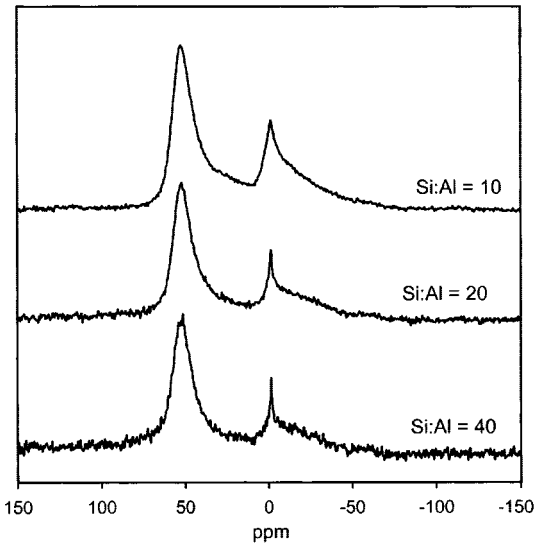


**Fig. 9** $^{27}$Al MAS NMR spectra of calcined aluminosilicate monoliths MO-SiAl*x*B30 prepared with various molar Si : Al ratios.

stability of aluminosilicate monoliths is improved compared to purely siliceous analogues.

The degree of aluminium incorporation into the framework can be assessed using $^{27}$Al MAS NMR. Fig. 9 illustrates the NMR spectra of the calcined aluminosilicate materials obtained with B30 and Si : Al ratios of 40, 20, 10. Analysis of the spectra suggests that most of all the aluminium observed is tetrahedrally co-ordinated, represented by the sharp peak at $\delta$ 52. Nevertheless, the appearance of a second sharp peak with a chemical shift at $\delta$ *ca.* 0 ppm and attributed to octahedrally co-ordinated aluminium indicates that extraframework Al is also present in the calcined samples. The relative intensity of tetrahedral and octahedral signals increases a little upon decreasing the Si : Al ratio. Thus the absolute amounts of the two aluminium types and their relative proportions undergo some changes when moving from MO-SiAl40*B30* to MO-SiAl10*B30*. For a quantitative comparison of the signals, one has to consider that $^{27}$Al has a spin greater than one half and it possesses a quadrupole moment.[58] The different environments in which aluminium occurs in the calcined monolithic nanostructures should have an impact on their surface acidity. Aluminosilicates usually display strong Brønsted acidity in addition to Lewis acid sites which are important for surface catalysis. For example, the condensation of $Si(OH)_4$ units with $(H_2O)Al(OH)_3$ units may produce a strong Brønsted acid in the form of 'bridging' Si(OH)Al hydroxy groups. It is also possible to enhance the Lewis-type acidity by creating extraframework aluminium during calcination. The presence of octahedrally co-ordinated Al in increasing amounts has been mentioned above. XRD provides evidence for an increase in disorder in the amorphous pore walls as Al is incorporated, resulting in less symmetric environments of the silicon and aluminium atoms. In consequence, the heterogeneity of acid site distribution is expected to be significant and it probably increases with decreasing Si : Al ratio.

The number and strength of the surface acids can be studied by the chemisorption of bases such as ammonia or pyridine.[9,59–64] Thermoprogrammed desorption of ammonia ($NH_3$ TPD) was used in the present study for the evaluation of surface acidity of aluminosilicate monoliths. The first important parameter inferred from the analysis of the TPD results is the amount of ammonia, $\Gamma_{IR}$, irreversibly adsorbed at 273 K and then removed from the surface by thermal treatment in the temperature range from 273 to 873 K. The value of $\Gamma_{IR}$ divided by the corresponding surface area, $S_{BET}$, can be identified with the density of surface acid sites per unit surface area of the solid substrate, $n_{acid}$. Such density parameters calculated for monolithic silica MO-Si*B30* and three aluminosilicates MO-SiAl40*B30*, MO-SiAl20*B30*, and MO-SiAl10B*30* are collected in Table 3. The total acidity value of purely siliceous monoliths is very small. The incorporation of aluminium into the monolithic nanostructure generates surface acid sites of increasing overall site density as the aluminium content is enhanced. The value of $n_{acid}$ is not a linear function of the total amount of Al present in the calcined samples, which points to heterogeneity of surface acid sites.

In the $NH_3$ TPD method, thermal stability of the adsorbed ammonia species is sometimes related to the strength of ammonia bonding. For example, temperature may be regarded as the direct measure of the strength of the acid sites exposed on the solid surface. This correlation should be treated with caution as the different diffusion rates of ammonia in porous solids can affect the results. It is probably adequate only for solid samples of the same kind, which do not evolve structurally and texturally during heating.[9,64] The strength distributions of acid sites in the three aluminosilicate monoliths templated with B30 were calculated from the $NH_3$ TPD results. Fig. 10*a* shows the amounts of ammonia desorbed from a unit surface area in five equal temperature ranges. The acid sites in MO-SiAl*x*B30 materials are clearly heterogeneous, with dominating moderate strengths. The numbers of sites of each kind increase with decreasing Si : Al ratio. The distributions in Fig. 10*b* present the fractions of acid sites in each sample belonging to different strength categories. They illustrate how the relative proportions between the various sites are modified upon increasing the amount of Al incorporated into nanostructured monoliths. Compared to MO-SiAl40*B30*, sample MO-SiAl20*B30* is enriched with moderate and strong sites at the expense of weaker acidities. It is easy to conclude that the mean strength of acid sites should increase from Si : Al = 40 to

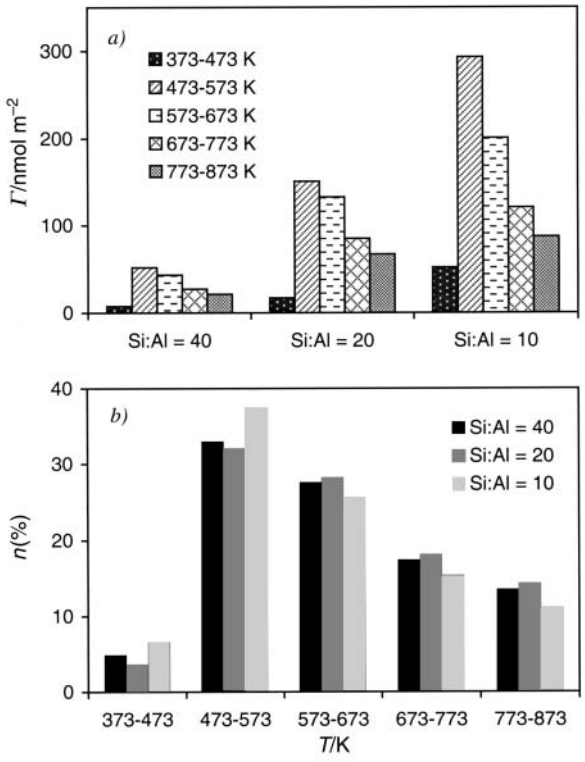


**Fig. 10** TPD strength distributions of acid sites for calcined aluminosilicate monoliths MO-SiAl*x*B30 prepared with various molar Si : Al ratios: *a*) the amounts of ammonia molecules, desorbed from a unit surface area of a given material in five temperature ranges, as functions of the sample type, *b*) the fraction of acid sites in each sample belonging to the five strength categories.

Si : Al = 20. When the Si : Al ratio is decreased to 10, the proportions are markedly turned in favour of weak acid sites. In consequence, the mean acid strength may equally well decrease when passing from MO-SiAl20*B30* to MO-SiAl10*B30*. The results of the flow-microcalorimetry study of ammonia chemisorption illustrate well this tendency.

The mean strength of acid sites was determined for the three aluminosilicate materials based on the continuous-flow method described in detail elsewhere.[64] In each case, ammonia adsorption at 373 K appeared to be partly reversible. The differences in the amount adsorbed and in the integral heat evolved between adsorption and desorption cycles gave the quantity of ammonia irreversibly adsorbed, $\Gamma_{IR}$, and the integral heat of irreversible adsorption, $Q_{IR}$. Ultimately, quantities $\Gamma_{IR}$ and $Q_{IR}$ provided direct access to the integral molar heat of ammonia chemisorption, $q_{IR}$, considered as the measure of the mean strength of acid sites. The following values of $q_{IR}$ were obtained: 98 kJ mol$^{-1}$, MO-SiAl40*B30*; 123 kJ mol$^{-1}$, MO-SiAl20*B30*; 112 kJ mol$^{-1}$, MO-SiAl10*B30*. These results clearly show that, although the incorporation of aluminium into monolithic materials causes the strength of surface acid sites to increase, changing the proportion of strong to weak sites induces a decrease in the mean acid strength for smaller Si : Al values.

### Effect of surfactant type

The direct liquid-crystal templating approach was applied to prepare monolithic aluminosilicates with a Si : Al ratio of 20 using various polyoxyethylated non-ionic structure-directing agents in high-concentration surfactant solutions (about 50 wt%).

Fig. 11 shows nitrogen adsorption–desorption isotherms measured at 77 K on a representative aluminosilicate series prepared using dodecylphenol-*n*EO templates. All curves are characteristic of fine pore adsorbents, with the beginning of the adsorption plateau region being shifted towards lower relative pressures compared to MO-SiAl*xB30* materials (see Fig. 8). Therefore, the mean pore diameter is also expected to be smaller. The effect becomes more pronounced as the number of EO units increases. Furthermore, the addition of ethylene groups to the POE chain causes the $N_2$ amount adsorbed at the plateau to diminish. Here the adsorption phenomenon is completely reversible. Similar-shaped curves were obtained for

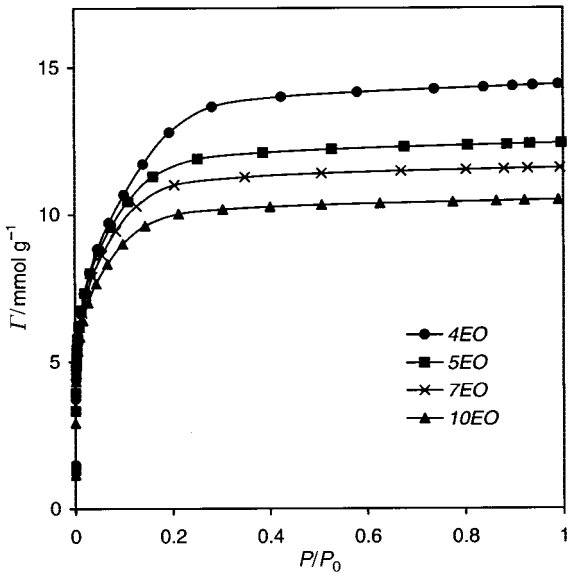


**Fig. 11** Effect of the polyoxyethylene chain length of the structure-directing agent on the nitrogen adsorption properties of the resulting aluminosilicate monoliths MO-SiAl20*DPEn* after removal of the template by calcination.

**Table 4** Surface area and porous structure parameters of aluminosilicate monoliths MO-SiAl20*TA* prepared using different polyoxyethylenated templates

| Surfactant template | $S_{BET}$/ m$^2$ g$^{-1}$ | $S_{mes}$/ m$^2$ g$^{-1}$ | $V_{mes}$/ cm$^3$ g$^{-1}$ | $d_p$/ nm | $V_{mic}$/ cm$^3$ g$^{-1}$ |
|---|---|---|---|---|---|
| *Oxyethylated alkylphenols* | | | | | |
| OPE10 | 757 | 511 | 0.23 | 1.8 | 0.09 |
| NPE4 | 988 | 688 | 0.37 | 2.1 | 0.08 |
| NPE5 | 927 | 687 | 0.34 | 2.0 | 0.08 |
| NPE8 | 854 | 628 | 0.29 | 1.8 | 0.08 |
| NPE10 | 834 | 572 | 0.27 | 1.9 | 0.09 |
| NPE12 | 791 | 550 | 0.25 | 1.8 | 0.09 |
| DPE4 | 1043 | 712 | 0.43 | 2.4 | 0.07 |
| DPE5 | 955 | 662 | 0.35 | 2.1 | 0.08 |
| DPE7 | 880 | 595 | 0.31 | 2.1 | 0.09 |
| DPE10 | 830 | 558 | 0.28 | 2.0 | 0.08 |
| *Lauryl ether-nEO* | | | | | |
| DE2 | 1152 | 737 | 0.56 | 3.0 | 0.06 |
| DE4 | 1070 | 702 | 0.46 | 2.6 | 0.07 |
| DE8 | 888 | 615 | 0.33 | 2.1 | 0.08 |
| *Montanox* | | | | | |
| M20 | 511 | 329 | 0.24 | 3.0 | 0.09 |
| M80 | 584 | 429 | 0.31 | 2.9 | 0.07 |
| M85 | 719 | 464 | 0.38 | 3.3 | 0.08 |

other template families, namely nonylphenol-*n*EO, octylphenol-10EO and lauryl ether-*n*EO. The analysis of the adsorption isotherms, based on the model described previously, allows estimates of the BET specific surface area and pore structure parameters to be made. They are given in Table 4. For oxyethylated alkylphenol and lauryl ether-*n*EO non-ionics used as structure-directing agents, the values of $S_{BET}$, $S_{mes}$, $V_{mes}$ and $d_p$ decrease with increase in the number of EO units at constant hydrophobic chain length. There is a small increase in the micropore volume when the length of the POE chain is increased. However, the trends become less pronounced for long-POE-chain members. If the number of EO units is greater than *ca.* 5, the mean pore diameter of aluminosilicate monoliths remains almost unchanged.

Alkyl homologues with low ethylene oxide content below 5 units are usually water-insoluble and show a propensity to form lamellar liquid-crystalline phases at concentrations near 50 wt% at ambient temperature.[33] In extended lamellar sheets, the arrangement of surfactant molecules is characterised by strong chain–chain and head–head interactions and the cross-sectional area per molecule reaches its minimum value. Lamellar mesophases also contain less water than hexagonal liquid-crystalline phases. It seems that POE chains located on the outside of the sheets may adopt specific orientations depending on the number of EO units. Close-packed hydrophilic head-groups with 2 EO units are presumably oriented perpendicular to the lamellar domains, thereby contributing directly to the effective size of the templating objects. When the number of EO units is increased, the ultimate orientation of the POE chains is the outcome of two opposing effects. On the one hand, their parallel orientation with respect to the lamellar sheets is preferred in response to specific interactions between the growing inorganic clusters and the surfactant head-groups during solidification of the inorganic matrix. For example, the adsorption of n-alkylphenylpolyethylene glycol and n-alkylpolyethylene glycol non-ionic surfactants onto silica involves the formation of hydrogen bonds between surface silanol groups and the long POE chains.[65] On the other hand, the order parameter for hydrophobic tails in lamellar phases discourages such conformation changes. With the POE chains increasingly tilted with respect to the water–aggregate interface, the template size decreases with increasing number of EO units, accounting for the changes observed in the mean pore diameter of the aluminosilicate monoliths.

Further oxyethylenation of surfactant units leads to an

increase in solubility and the resulting non-ionic amphiphiles rather tend to form hexagonal mesophases under the same conditions. Order parameters for hexagonal liquid-crystalline phases are reduced to half of those for lamellar phases due to the different alignment of the interface between hydrophobic and hydrophilic domains with respect to the liquid crystal uni-axis. Under such circumstances, long POE chains can be oriented parallel to the interface during the polycondensation process. In consequence, they do not contribute directly to the template size but can influence it through some subtle changes in the aggregation number (*e.g.* increase in the cross-sectional area of the head-group and in the asymmetry of the non-ionic aggregate). It is also true that the reliable definition of head-group becomes increasingly difficult in progressing through the series. Since commercial polyoxyethylene non-ionics are mixtures containing POE chains with different numbers of EO units clustered about some mean value, their influence on the templating mechanism is weaker than that of single-species materials containing the same hydrophobic moiety and with oxyethylene content corresponding to the mean value. Heterogeneity of internal nanostructure in monolithic materials certainly increases with lengthening the POE chain of the amphiphilic structure-directing agent.

For 10 EO units in the POE chain of the template (OPE10, NPE10 and DPE10 surfactants), the mean pore diameter of aluminosilicate monoliths increases with increasing length of the hydrophobic tail, which reflects the larger size of the template objects.

Three polyoxyethylenated derivatives of sorbitol belonging to the Montanox family give particular mesoporous materials. The corresponding isotherms of nitrogen, plotted in Fig. 12, are of type IV with a hysteresis loop. The shape of the latter is consistent with the presence of 'ink-bottle' pores having a narrow entrance and wide interior. The neck diameter is probably of the same order of magnitude in the three materials studied, because the pores begin to empty at the same relative pressure. It is interesting to note that, using similar sorbitan-derivatised templates at much lower amphiphile concentrations, Prouzet *et al.*[66] obtained MSU-*X* type powdered silica, with pore sizes in the 3–4 nm range and a significant textural porosity in the 9–20 nm range. No interparticle porosity can be observed for monolithic samples. Here the internal nanostructure can be seen as the regular pore network with a series of interconnected pore spaces and narrow channels linking the pores to the outer surface of the material. The specific surface area and pore structure parameters calculated from the adsorption branches of the isotherms are given in Table 4. The nitrogen adsorption isotherms for Montanox-based monolithic aluminosilicates differ in shape from the curves measured on monolithic silicas prepared using the same structure directors (see Fig. 4). The nanostructure of the former is dominated by larger mesopores. The values of $S_{BET}$, $S_{mes}$, $V_{mes}$ and $d_p$ increase with increasing number of alkyl substituents in the template structure. Changes in the length of such a substituent do not affect much the 'average' pore network. It may reasonably be argued that the degree of molecular ordering in the liquid crystalline phases of these amphiphiles, and so the pore structure of the resulting monoliths, is determined to a greater extent by the bulky head-groups than by the hydrophobic moieties.

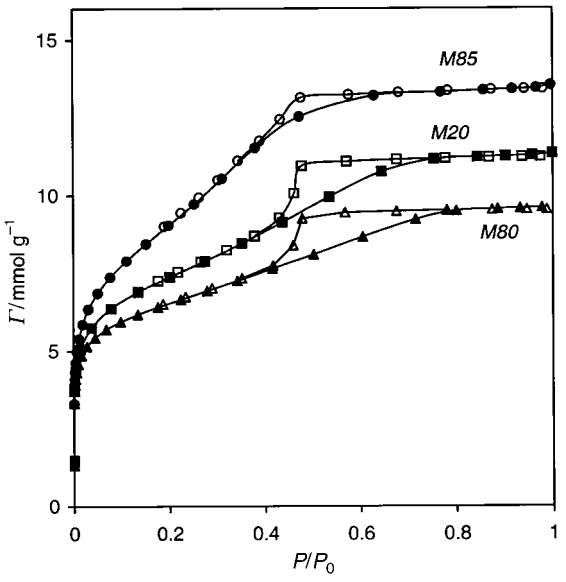


**Fig. 12** Adsorption–desorption isotherms of nitrogen at 77 K onto calcined aluminosilicate monoliths MO-SiAl20*TA* prepared using structure-directing agents from the Montanox series.

### Effect of the environment of the reaction mixture: temperature and additives

Although surfactant phase behaviour is mainly correlated with molecular structure, the temperature of the aqueous phase and the presence of additives may modify to a great extent surfactant solubility and mesophase formation. The regular pore network of MSU-X silicas prepared using Tergitol 15-S-12 as structure director in low-concentration surfactant solutions was shown to be sensitive to the synthesis temperature.[28] An increase in temperature in the range from 25 to 65 °C afforded highly mesostructured silicas with a greater pore diameter and a smaller BET surface area. These trends were attributed to a decrease in hydrophilicity and overall size of the POE chains with increasing temperature, thereby resulting in a decreased micelle curvature and an increased size of the hydrophobic core of the surfactant aggregates.

In the present case, for surfactant templates B30 and T9, raising the synthesis temperature from 4 to 50 °C generally causes the specific surface area, the mesopore volume and the mean pore diameter to decrease. Low-temperature monoliths are predominantly mesoporous, whereas those prepared at higher temperatures become increasingly microporous, as can be deduced from the parameters collected in Table 5. These materials are produced in high-concentration template solutions through the liquid-crystalline phase templating mechanism. It is known that processes such as heating or cooling cut across phase diagrams and passing through a boundary from one phase to another can involve quite dramatic changes in the geometry of surfactant aggregation. For example, transformations from the hexagonal phase to the lamellar, cubic or even micellar $L_1$ phases are possible, depending on the overall surfactant concentration and the increase of temperature.[33] On cooling near 0 °C, formation of hydrated surfactant crystals can be even induced. Using evidence from X-ray diffraction experiments, phase transformations are to be excluded in the present case. More likely, a decrease in temperature from 30 to 4 °C diminishes the translational freedom of surfactant units within aggregates and may also impose restrictions on the motion of water molecules. Under such conditions, POE chains in 'frozen' rod-like conformation adopt an orientation perpendicular to the aggregate–water interface and contribute considerably to the size of the templating aggregates, which determine the framework pore size. Other changes that may affect the solidification mechanism are: increased viscosity of the mesophase, slower hydrolysis of TEOS or slower polycondensation of silicic acid. When the $T_p$ temperature is increased to 50 °C, the order parameter for alkyl chains in the hydrophobic domains of the mesophase is reduced and, simultaneously, EO units are partially dehydrated. The POE chains are oriented parallel to the surfactant–silica interface and the size of templating aggregates is diminished.

It has been already shown above that solubilisate additives

**Table 5** Temperatures of the different stages in the synthesis of MO-SiAl20*TA* materials and their impact on the surface area and porous structure parameters

| Surfactant template | $T_p$/°C | $T_v$/°C | $T_d$/°C | $S_{BET}$/m$^2$ g$^{-1}$ | $S_{mes}$/m$^2$ g$^{-1}$ | $V_{mes}$/cm$^3$ g$^{-1}$ | $d_p$/nm | $V_{mic}$/cm$^3$ g$^{-1}$ |
|---|---|---|---|---|---|---|---|---|
| T9 | 4 | 4 | 4 | 872 | 594 | 0.33 | 2.2 | 0.08 |
| T9 | 30 | 25 | 25 | 800 | 425 | 0.19 | 1.8 | 0.10 |
| T9 | 50 | 25 | 50 | 768 | 405 | 0.17 | 1.7 | 0.09 |
| B30 | 4 | 4 | 4 | 1086 | 665 | 0.50 | 3.0 | 0.06 |
| B30 | 30 | 25 | 25 | 999 | 661 | 0.43 | 2.6 | 0.06 |
| B30 | 50 | 25 | 50 | 903 | 626 | 0.33 | 2.1 | 0.08 |
| B30 | 30 | 25 | 50 | 878 | 596 | 0.31 | 2.1 | 0.08 |

$T_p$: temperature at which the reagents are mixed during synthesis; $T_v$: temperature of the vacuum treatment; $T_d$: temperature of the drying stage.

may significantly increase the mean pore size of monolithic silica. To study the effect of solubilisate concentration on the templating mechanism, increasing amounts of 1,3,5-trimethylbenzene (TMB) were added to the reaction mixture during preparation of monolithic aluminosilicates with a Si : Al ratio of 20 using B30 as the template molecule. The solubilisate was added in a manner to obtain molar Si : TMB ratio ranging from 0.67 to 2. After removal of the organic template by calcination, the existence of mesopore network was detected, as exemplified by the type IV isotherms of nitrogen in Fig. 13. The resulting values of $S_{BET}$, $S_{mes}$, $V_{mes}$, $d_p$ and $V_{mic}$ are collected in Table 6. The mean pore diameter and the mesopore volume increase markedly with increasing TMB content. Changes in the BET specific surface area are relatively small. The mean pore diameter of a purely siliceous monolith prepared using the same template at a constant Si : TMB ratio of 1 is smaller by about 0.4 nm. As evidenced by the increased X-ray Bragg spacing, the average wall thickness of the mesoporous materials synthesised in the presence of TMB is markedly larger, indicating their enhanced thermal and mechanical stability.

In polyoxyethylenated non-ionics, polarisable hydrocarbons were shown to be solubilised between the polyoxyethylene chains of the hydrophilic head-groups.[53] Since the effective cross-sectional area of the latter increases, the micelle in aqueous medium becomes increasingly asymmetrical, with the result that the volume of the inner core increases relative to that of the outer portion. Solubilisation of additional polarisable material may be either deep in the micellar palisade layer or

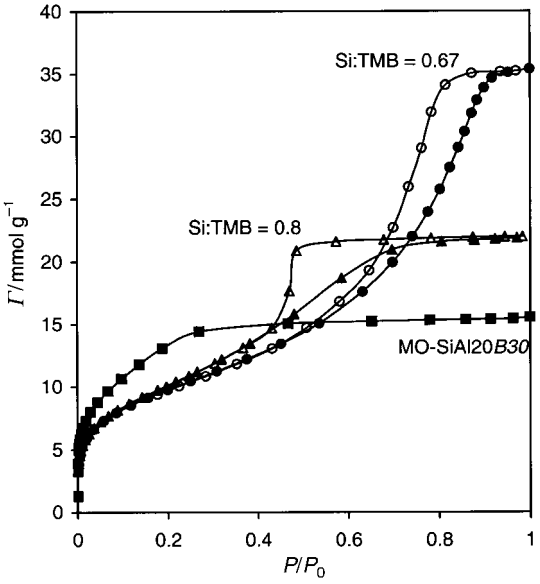


**Fig. 13** Effect of the addition of 1,3,5-trimethylbenzene (TMB) to the reaction mixture on the nitrogen adsorption properties of the resulting aluminosilicate monoliths MO-SiAl20*B30* after removal of the organic template by calcination. The molar Si : TMB ratios are also indicated.

**Table 6** Effect of the addition of 1,3,5-trimethylbenzene (TMB) to the reactive mixture on the surface area and porous structure parameters of porous silicate and aluminosilicate monoliths prepared using B30 as the surfactant template

| Si : Al molar ratio | Si : TMB molar ratio | $S_{BET}$/ m$^2$ g$^{-1}$ | $S_{mes}$/ m$^2$ g$^{-1}$ | $V_{mes}$/ cm$^3$ g$^{-1}$ | $d_p$/ nm | $V_{mic}$/ cm$^3$ g$^{-1}$ |
|---|---|---|---|---|---|---|
| ∞ | 1 | 867 | 616 | 0.52 | 3.4 | 0.05 |
| 20 | 2 | 902 | 608 | 0.45 | 3.0 | 0.05 |
| 20 | 1 | 906 | 617 | 0.58 | 3.8 | 0.05 |
| 20 | 0.8 | 829 | 521 | 0.68 | 5.2 | 0.07 |
| 20 | 0.67 | 781 | 773 | 1.18 | 6.1 | 0.00 |

even located in the inner core of the micelle and, in consequence, the increase in the diameter of an aggregate is even more significant. These changes generalised to liquid-crystalline phases account for the increased pore size and pore volume. Larger mesopores begin to dominate in the calcined materials. For Si : TMB ratios below 1, hysteresis loops are present in the nitrogen adsorption–desorption isotherms (see Fig. 13). In low-concentration surfactant solutions, continued addition of non-polar substance may result in the conversion of the hexagonal micelle to a normal lamellar micelle and eventually to an inverted lamellar micelle. In rigid liquid-crystalline structures, the phenomenon should be limited by the space available for the solubilisate. For a sample prepared with a Si : TMB ratio lower than 0.67, the separation of a thin opaque layer was observed after calcination. This opaque layer was less ordered but had an average pore diameter similar to that of the base material.

In a final stage, the effect of lithium nitrate addition on the interfacial properties of monolithic materials was investigated. The mesophase templating approach to the preparation of monolithic silica was applied based on non-ionic T9 as the structure-directing agent. The nitrogen adsorption–desorption isotherms referring to materials prepared with different Si : Li molar ratios are shown in Fig. 14. The corresponding BET surface area and pore structure parameters are given in Table 7. The addition of small quantities of Li salt induces small changes in the isotherm shape. Further addition of electrolyte produces isotherms with a hysteresis loop, characteristic of materials containing larger mesopores. An increase in the lithium content causes a great increase in the mean pore diameter from 2.7 nm (Si : Li = ∞) to 5.1 nm (Si : Li = 5). This increase in the pore size is accompanied by a considerable decrease in the specific surface area and pore volume of the monolithic materials studied. Murakata and co-workers[67] observed an increase in the pore size of silica gel on addition of various salts. Sierra *et al.*[29] interpreted this effect as a result of interaction between alkali metal cations and head-groups of the non-ionic surfactant. Cations are able to break hydrogen bonding between hydrophilic moieties and water dipoles, thereby producing surfactant units in more extended conformations. $Li^+$ ions have a high affinity towards the EO units and can easily displace water that hydrates the head-groups.

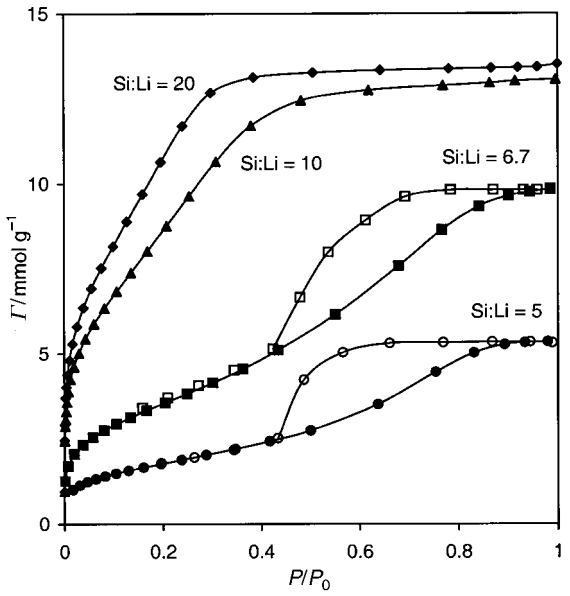


**Fig. 14** Effect of the addition of lithium nitrate to the reaction mixture on the nitrogen adsorption properties of calcined monolith MO-Si*B30*. The molar Si : Li ratios are also indicated.

**Table 7** Effect of lithium ion incorporation into the silica matrix, on surface area and porous structure parameters of monolithic samples prepared using T9 as the surfactant template

| Si : Li molar ratio | $S_{BET}$/ $m^2 g^{-1}$ | $S_{mes}$/ $m^2 g^{-1}$ | $V_{mes}$/ $cm^3 g^{-1}$ | $d_p$/ nm | $V_{mic}$/ $cm^3 g^{-1}$ |
|---|---|---|---|---|---|
| ∞ | 955 | 617 | 0.41 | 2.7 | 0.04 |
| 20 | 943 | 565 | 0.42 | 2.9 | 0.05 |
| 10 | 766 | 431 | 0.40 | 3.7 | 0.04 |
| 6.7 | 293 | 275 | 0.33 | 4.7 | 0.00 |
| 5 | 147 | 140 | 0.18 | 5.1 | 0.00 |

For high Li contents, additional arguments should be put forward to explain the effect of salt addition. The resulting monolithic materials have unexpectedly small surface areas and pore networks with a broad distribution of pore sizes. The templating aggregates seem to have different structures in concentrated electrolyte solutions. This conclusion is consistent with the reduced surfactant solubility when the hydrophobic moiety is salted out by the presence of strongly polarisable ions. Furthermore, the depletion of water dipoles in the system due to strong water–ion interactions may slow down the hydrolysis of TEOS and decrease the dissolution of the silicic acid in the aqueous domains of the existing surfactant phases. Consequently, the solidification of the inorganic matter occurs around large surfactant structures of irregular sizes and shapes.

## Conclusions

The direct liquid crystal templating approach to surfactant-assisted synthesis of porous silica affords monolithic materials, in which a regular pore network is combined with a high surface area. Solidification of the inorganic matter in lyotropic liquid-crystalline phases allows the internal nanostructure to be easily controlled through the factors determining the geometry of the parental mesophase. The molecular structure and concentration of the template, as well as the temperature of the synthesis, are the main parameters that determine the general disposition of mesomorphic phases in the phase diagram and, consequently, influence the porosity of the resulting materials. The pore size is adjusted during the synthesis in reponse to specific interactions between the hydrophilic head-groups and the growing inorganic clusters. Addition of group I metal salts or organic solubilisates to the reaction mixture may also produce marked changes in the pore structure. With commercially available oxyethylated non-ionics as cheap structure-directing agents used in high-concentration surfactant solutions, the crystalline-like pore structure appears to be somewhat disordered due to the inherent polydispersity of the template material.

The templating mechanism may be extended to the preparation of aluminosilicate monoliths possessing a regular pore network with a narrow distribution of pore sizes. The increased thickness of the pore walls contributes to improve the thermal and mechanical stability of these materials compared to the purely siliceous homologues. The incorporation of aluminium into monolithic silica greatly enhances the overall surface acidity, without compromising the large surface area and pore volume.

Generally, the mean pore diameter of silica and aluminosilicate monoliths ranges from 2 nm to 4 nm. It increases with increasing length of the hydrophobic tail and decreasing number of oxyethylene units in the non-ionic template. Materials with much larger pores are obtained when adding lithium nitrate or 1,3,5-trimethylbenzene to the reaction mixture.

*Note added at proof*: while this article was in press, Coleman and Attard (*Microporous Mesoporous Mater.*, 2001, **44**, 73) reported the preparation of mesoporous silicas from liquid crystal phases of non-ionic surfactant Brij 56. These authors show that hexagonally ordered phases can be obtained. Similar results are reported in the present article, except that less well-ordered materials are obtained; this difference probably lies in the use of industrial surfactants of other origins and with different chain lengths and number of ethylene oxide units.

## References


1 F. H. Dickey, *Proc. Natl. Acad. Sci., USA*, 1949, **35**, 227.
2 G. Wulff, A. Sarhan and K. Zabrocki, *Tetrahedron Lett.*, 1973, 4329.
3 S. L. Lawton and W. J. Rohrbaugh, *Science*, 1990, **247**, 1319.
4 T. Yanagisawa, T. Shimizu, K. Kuroda and C. Kato, *Bull. Chem. Soc. Jpn.*, 1990, **63**, 988.
5 C. T. Kresge, M. E. Leonowicz, W. J. Roth, J. C. Vartuli and J. S. Beck, *Nature*, 1992, **359**, 710.
6 S. L. Burkett and M. E. Davis, *J. Phys. Chem.*, 1994, **4647**, 98; S. L. Burkett and M. E. Davis, *Chem. Mater.*, 1995, **7**, 920; S. L. Burkett and M. E. Davis, *Chem. Mater.*, 1995, **7**, 1453.
7 N. K. Raman, M. K. Anderson and C. J. Brinker, *Chem. Mater.*, 1996, **8**, 1682.
8 A. Sayari and P. Liu, *Microporous Mater.*, 1997, **12**, 149.
9 D. J. Jones, G. Aptel, M. Brandhorst, M. Jacquin, J. Jiménez-Jiménez, A. Jiménez-Lopez, P. Maireles-Torres, I. Piwonski, E. Rodriguez-Castellon, J. Zajac and J. Rozière, *J. Mater. Chem.*, 2000, **10**, 1957.
10 J. S. Beck, J. C. Vartuli, W. J. Roth, M. E. Leonowicz, C. T. Kresge, K. D. Schmitt, C. T.-W. Chu, D. H. Olson, E. W. Sheppard, S. B. McCullen, J. B. Higgins and J. L. Schlenker, *J. Am. Chem. Soc.*, 1992, **114**, 10834.
11 O. Franke, G. Schulz-Ekloff, J. Rathousky, J. Starek and A. Zukal, *J. Chem. Soc., Chem. Commun.*, 1993, 724.
12 A. Monnier, F. Schüth, Q. Huo, D. Kumar, D. Margolese, R. S. Maxwell, G. D. Stucky, M. Krishnamurty, P. Petroff, A. Firouzi, M. Janicke and B. F. Chmelka, *Science*, 1993, **261**, 1299.
13 P. J. Branton, P. G. Hall, K. S. W. Sing, H. Reichert, F. Schüth and K. K. Unger, *J. Chem. Soc., Faraday Trans.*, 1994, **90**, 2965.
14 P. L. Llewellyn, Y. Grillet, F. Schüth, H. Reichert and K. K. Unger, *Microporous Mater.*, 1994, **3**, 345.
15 J. S. Beck, J. C. Vartuli, G. J. Kennedy, C. T. Kresge, W. J. Roth and S. E. Schramm, *Chem. Mater.*, 1994, **6**, 1816.
16 G. Fu, C. A. Fyfe, W. Schwieger and G. T. Kokotailo, *Angew. Chem., Int. Ed. Engl.*, 1995, **34**, 1499.
17 Zh. Luan, C.-F. Cheng, W. Zhou and J. Klinowski, *J. Phys. Chem.*, 1995, **99**, 1018.
18 R. B. Borade and A. Clearfield, *Catal. Lett.*, 1995, **31**, 267.

19 H. Y. Zhu, X. S. Zhao, G. Q. Lu and D. D. Do, *Langmuir*, 1996, **12**, 6513.
20 M. J. Meziani, J. Zajac, D. J. Jones, J. Rozière and S. Partyka, *Langmuir*, 1997, **13**, 5409.
21 I. Piwonski, J. Zajac, D. J. Jones, J. Rozière and S. Partyka, *J. Mater. Chem.*, 1998, **8**, 17.
22 L. Y. Chen, S. Jaenicke and G. K. Chuah, *Microporous Mater.*, 1997, **12**, 323.
23 C. G. Göltner and M. Antonietti, *Adv. Mater.*, 1997, **9**, 431.
24 Q. Huo, D. I. Margolese, U. Ciesla, P. Feng, T. E. Gier, P. Sieger, R. Leon, P. M. Petroff, F. Schuth and G. D. Stucky, *Nature*, 1994, **24**, 317.
25 P. T. Tanev and T. J. Pinnavaia, *Science*, 1995, **267**, 865.
26 P. Behrens, *Angew. Chem., Int. Ed. Engl.*, 1996, **35**, 515.
27 S. A. Bagshaw, E. Prouzet and T. J. Pinnavaia, *Science*, 1995, **269**, 1242.
28 E. Prouzet and T. J. Pinnavaia, *Angew. Chem., Int. Ed. Engl.*, 1997, **36**, 516.
29 L. Sierra and J. L. Guth, *Microporous Mesoporous Mater.*, 1999, **27**, 243.
30 D. Zhao, J. Feng, Q. Huo, N. Melosh, G. H. Fredrickson, B. F. Chmelka and G. D. Stucky, *Science*, 1998, **279**, 548.
31 V. Luzzati, H. Mustacchi and A. Skoulios, *Discuss. Faraday Soc.*, 1958, **25**, 43.
32 G. J. T. Tiddy, *Phys. Rep.*, 1980, **57**, 1.
33 D. J. Mitchell, G. J. T. Tiddy, L. Waring, T. Bostock and M. P. McDonald, *J. Chem. Soc., Faraday Trans. 1*, 1983, **79**, 975.
34 N. Casillas, J. E. Puig, R. Olayo, T. J. Hart and E. I. Franses, *Langmuir*, 1989, **5**, 384.
35 G. S. Attard, M. Edgar, J. W. Emsley and C. G. Göltner, in *Liquid Crystals for Advanced Technologies*, ed. T. J. Bunning, S. H. Chen, W. Hawthorne, T. Kajiyama and N. Koide, MRS, Pittsburgh, 1996.
36 G. S. Attard, J. C. Glyde and C. G. Göltner, *Nature*, 1995, **378**, 366.
37 G. S. Attard, M. Edgar and C. G. Göltner, *Acta Metall. Mater.*, 1998, **46**, 751.
38 S. E. Friberg, C.-C. Yang, R. Goubran and R. E. Partch, *Langmuir*, 1991, **7**, 1103.
39 S. E. Friberg, C.-C. Yang and J. Sjöblom, *Langmuir*, 1992, **8**, 372.
40 L. Auvray, A. Ayral, T. Dabadie, L. Cot, C. Guizard and J. D. F. Ramsay, *Faraday Discuss. Chem. Soc.*, 1995, **101**, 235.
41 B. Ammundsen, G. Burns, D. J. Jones and J. Rozière, *J. Sol–Gel Sci. Technol.*, 1997, **8**, 331.
42 C. G. Göltner, S. Henke, M. C. Weissenberg and M. Antonietti, *Angew. Chem., Int. Ed.*, 1998, **37**, 613.
43 S. H. Tolbert, A. Firouzi, G. D. Stucky and B. F. Chmelka, *Science*, 1997, **278**, 264.
44 Y. Wei, D. Jin, T. Ding, W.-H. Shih, Z. D. Cheng and Q. Fu, *Adv. Mater.*, 1998, **3**, 313.
45 Y. Wei, J. Xu, H. Dong, J. H. Dong, K. Qiu and S. A. Jansen-Varnum, *Chem. Mater.*, 1999, **11**, 2023.
46 N. A. Melosh, P. Lipic, F. S. Bates, F. Wudl, G. D. Stucky, G. H. Fredrickson and B. F. Chmelka, *Macromolecules*, 1999, **32**, 4332.
47 N. A. Melosh, P. Davidson, P. Feng, D. J. Pine and B. F. Chmelka, *J. Am. Chem. Soc.*, 2000.
48 P. Feng, X. Bu and D. J. Pine, *Langmuir*, 2000, **16**, 5304.
49 P. Feng, X. Bu, G. D. Stucky and D. J. Pine, *J. Am. Chem. Soc.*, 2000, **122**, 994.
50 R. G. Laughlin, in *Advances in Liquid Crystals*, ed. G. H. Brown, Academic Press, New York, 1978, p. 41.
51 M. J. Rosen, *Surfactants and Interfacial Phenomena*, Wiley, New York, 1989.
52 S. J. Gregg and K. S. W. Sing, *Adsorption, Surface Area and Porosity*, Academic Press, London, 1982.
53 T. Nakagawa, in *Nonionic Surfactants*, ed. M. J. Schick, Marcel Dekker, New York, 1967, ch. 17.
54 R. Nagarajan, M. A. Chaiko and E. Ruckenstein, *J. Phys. Chem.*, 1984, **88**, 2916.
55 D. H. Everett, in *Characterisation of Porous Solids*, S. J. Gregg, K. S. W. Sing and H. F. Stoeckli, Soc. Chem. Ind., London, 1979; p. 229.
56 A. Saito and H. C. Foley, *AlChE J.*, 1991, **37**, 429.
57 W. W. Lukens Jr., P. Schmidt-Winkel, D. Zhao, J. Feng and G. D. Stucky, *Langmuir*, 1999, **15**, 5403.
58 C. Contescu, J. Jagiello and J. A. Schwarz, *Langmuir*, 1993, **9**, 1754.
59 A. Gervasini and A. Auroux, *J. Phys. Chem.*, 1993, **97**, 2628.
60 M. J. Meziani, J. Zajac, D. J. Jones, S. Partyka, J. Rozière and A. Auroux, *Langmuir*, 2000, **16**, 2262.
61 M. Busio, J. Jänchen and J. C. H. Van Hooff, *Microporous Mater.*, 1995, **5**, 211.
62 C.-Y. Chen, H.-X. Li and M. E. Davis, *Microporous Mater.*, 1993, **2**, 17.
63 R. Mokaya, W. Jones, L. Zhaohua, M. D. Alba and J. Klinowski, *Catal. Lett.*, 1996, **37**, 113.
64 J. Zajac, R. Dutartre, D. J. Jones and J. Rozière, *Thermochimica Acta*, 2001, in press.
65 J. S. Clunie and B. T. Ingram, in *Adsorption from Solution at the Solid–Liquid Interface*, ed. G. D. Parfitt and C. H. Rochester,, Academic Press, London, 1983, p. 105.
66 E. Prouzet, F. Cot, G. Nabias, A. Larbot, P. Kooyman and T. J. Pinnavaia, *Chem. Mater.*, 1999, **11**, 1498.
67 T. Murakata, S. Sato, T. Ohgawara, T. Watanabe and T. Suzuki, *J. Mater. Sci.*, 1992, **27**, 156.